Algebraic growth in a Blasius boundary layer: optimal and robust control by mean suction in the nonlinear regime

By SIMONE ZUCCHER[1]†, PAOLO LUCHINI[2]
AND ALESSANDRO BOTTARO[3]‡

[1]Dipartimento di Ingegneria Aerospaziale, Politecnico di Milano, Via La Masa 34, 20158 Milano, Italy

[2]Dipartimento di Ingegneria Meccanica, Università di Salerno, 84084 Fisciano, Italy

[3]Institut de Mécanique des Fluides de Toulouse, 34100 Toulouse, France

Optimal and robust control for the three-dimensional algebraically growing instability of a Blasius boundary layer is studied in the nonlinear regime. First, adjoint-based optimization is used to determine an optimal control in the form of a spanwise-uniform wall suction that attenuates the transient growth of a given initial disturbance, chosen to be the optimal perturbation of the uncontrolled flow. Secondly, a robust control is sought and computed simultaneously with the most disrupting initial perturbation for the controlled flow itself. Results for both optimal and robust control show that the optimal suction velocity peaks near the leading edge. In the robust-control case, however, the peak value is smaller, located farther downstream from the leading edge, and the suction profile is much less dependent on the control energy than in the optimal-control case.

1. Introduction

1.1. *The formation of streaks*

Transient growth of disturbances is a mechanism which appears to reconcile the seeming contrast between classical stability theory (based on the growth or decay of a single-mode perturbation) and experimental observations of the initial phases of transition in boundary layers, channels and pipes (cf. Schmid & Henningson 2001).

In the case of the Blasius boundary layer, it is by now accepted that more than one route to transition is possible: when free-stream disturbances are very small, transition is conceivably preceded by the exponential amplification of Tollmien–Schlichting waves. On the other hand, when somewhat larger perturbations are present, the near-wall region becomes populated by elongated streaks of low and high streamwise velocity. Arguably the most detailed recent experiments supporting this description have been conducted in Stockholm (cf. for example, Boiko *et al.* 1994; Westin *et al.* 1994; Matsubara & Alfredsson 2001) and Pasadena (cf. Kendall 1985, 1998).

---

† Present address: Mechanical and Aerospace Engineering, Arizona State University, Tempe AZ 85287, USA.

‡ Present address: DIAM, Università di Genova, Via Montallegro 1, 16145 Genova, Italy.

Early theory was able to explain the presence of the streaks on the basis of a physical argument, named the *lift-up effect* by Landahl (1980). Today, most attention has shifted to the fact that the linearized operator governing the amplification of infinitesimal disturbances is highly non-normal (Trefethen *et al.* 1993) and, as a consequence, significant transient amplification of non-modal disturbances can occur even in subcritical flow configurations. The study of solutions of the linearized stability equations has demonstrated that transient growth produces streaks (cf. the spatial theory by Luchini 1997, 2000, and Andersson, Berggren & Henningson 1998, 1999). In the course of recent developments, Zuccher, Bottaro & Luchini (2004) have identified the optimal initial perturbations that provide the largest amplification of the streaks in the nonlinear regime. It turns out that energy growth is significantly dependent on the spanwise scale of the streaks, and that, in the presence of large initial disturbance amplitudes, the most amplified streaks are more loosely spaced than in the linearized case.

1.2. *The control of streaks*

A free-stream perturbation impinging on the leading edge of a flat plate can cause transition if it is of the correct shape and amplitude. Although the steps that follow the growth of the streaks and that lead to transition are still the subject of debate and research (cf. Wu & Choudhari 2001), it is reasonable to argue that transition can be spatially delayed if the amplification of the streaks is hampered. In this paper, the wall boundary condition is employed to control the growth of the streaks. The term 'optimal control' is here used to denote the best way of controlling a certain initial perturbation. In the context of boundary-layer instabilities, the perturbation kinetic energy is usually taken as an indicator of the level of disturbances, so that the control can be optimized by requiring, for instance, the energy at the end of the plate (or the integral of the energy over the streamwise length) to be the lowest. One of the most classical and practically convenient means of affecting the flow, experimented upon since Prandtl's time, is applying suction at the wall (see Floryan & Saric 1979; Myose & Blackwelder 1991, 1995).

Previous work on transition delay has mainly considered suction/blowing distributions of the same wavenumber and frequency as the disturbance wave. This is, in fact, a necessary choice if the analysis is to be contained within the limits of a linear model. Bewley & Liu (1998) applied modern control theory to determine, in a linear framework and at a fixed Reynolds number, the vertical wall velocity oscillation capable of optimally counteracting waves and non-modal disturbances in plane channel flows. They also considered a form of control known as 'robust control', upon which we will dwell later. Cathalifaud & Luchini (2000) optimized the algebraic growth of streaks in boundary layers by blowing and suction at the wall. In their work, the boundary-layer equations linearized about the Blasius base flow are solved using the linear optimal perturbation as initial condition. Suction and blowing are applied at the wall, in the form of a given v-component of the perturbation velocity, and adjoint-based optimization is then employed to determine the most effective oscillating-suction distribution. Corbett & Bottaro (2001) studied the control of parallel temporal optimal perturbations under a pressure gradient via blowing/suction at the wall, using a cost function which combined a weighted sum of the terminal and average disturbance energy with the control effort; their base flow was a boundary layer described by Falkner–Skan–Cooke similarity solutions. All of these studies embody a concept known as 'cancellation control': the

spanwise-oscillating flow induced by the wall suction and blowing is optimized so as to cancel the perturbation linearly.

On the other hand, we can also resort to an alteration of the mean flow, of the type classically proposed for transition control (see Schlichting 1979, chap. 14). This kind of control is fundamentally different because it does not require any feedback; whereas the oscillating blowing and suction distribution of Cathalifaud & Luchini (2000) must be in phase with the external disturbance to be effective, a mean-flow modification acts independently of phase. On the other hand, its action mechanism is nonlinear, and only a nonlinear model can achieve its optimization. Recently, under the impulse of a European project dedicated to applying laminar-flow technology to transport aircrafts, the optimization of suction systems meant to delay transition over fins and nacelles of a large aircraft has been undertaken. Theoretical results in this framework have been reported by Pralits, Hanifi & Henningson (2002) and Airiau *et al.* (2003). Both groups, using an adjoint-based optimization of the solution of parabolized stability equations, found the optimal steady suction for the control of infinitesimal disturbances in incompressible flows.

The simplest approach to identifying the optimal control of a given flow is to impose the worst initial condition and then optimize the control. This procedure is indeed generally known by the name of 'optimal control'. However, on second thoughts, this does not really represent the most effective control, because the presence of the control makes the worst initial condition different. When the worst initial perturbation is computed in the presence of the control itself, which implies that both must be simultaneously optimized, 'robust control' is obtained, a rigorous analysis of which has been presented by Bewley, Temam & Ziane (2000) in the context of the Navier–Stokes system of equations. They established conditions on the initial data, the parameters in the cost functional and the regularity required of the flow field such that existence and uniqueness of the robust control can be proved. They considered both linear and nonlinear cases and proposed numerical algorithms based on the repeated computation of an adjoint field, but did not present any quantitative results.

1.3. *Goal of the present work*

The present study aims at providing the optimal and robust mean wall-suction distributions that most efficiently attenuate the growth of streaks through a modification of the mean flow. Such a result can only be obtained in the context of nonlinear equations. In addition, a nonlinear study will automatically take into account the results of Zuccher *et al.* (2004), that is, at large initial energy, a saturation state can be reached and the disturbance energy remains more or less constant with streamwise position in the final part of the plate, and also of any new mode interactions that might possibly be triggered by the control itself, thus spoiling the beneficial effects aimed for.

For this purpose, the velocity field is decomposed in a Fourier series along the spanwise direction, so that an arbitrary shape produced by nonlinear effects can be accounted for.

The worst initial condition (optimal perturbation) computed without control in Zuccher *et al.* (2004) will be optimally controlled using a spanwise-uniform wall suction velocity, obtaining the strongest reduction in disturbance energy. Robust optimal control will then be applied, by simultaneously computing the worst initial condition and the corresponding best control at the wall.

2. Problem formulation

The behaviour of steady streaky structures in the laminar flow past a flat plate can be studied by employing the three-dimensional incompressible boundary-layer equations, written below in conservative form:

$$
\left.
\begin{aligned}
u_x + v_y + w_z &= 0, \\
(uu)_x + (uv)_y + (uw)_z - u_{yy} - u_{zz} &= 0, \\
(uv)_x + (vv)_y + (vw)_z + p_y - v_{yy} - v_{zz} &= 0, \\
(uw)_x + (vw)_y + (ww)_z + p_z - w_{yy} - w_{zz} &= 0.
\end{aligned}
\right\}
\tag{2.1}
$$

The scaling of variables is the following: the streamwise coordinate x is normalized with the total length of the plate L, the wall-normal coordinate y and the spanwise coordinate z are made dimensionless with $\delta = Re^{-1/2}L = (\nu L/U_\infty)^{1/2}$, the streamwise velocity u is made dimensionless with respect to the outer velocity U_∞, whereas v and w (respectively wall-normal and spanwise components) are made dimensionless with respect to $Re^{-1/2}U_\infty$; Re is the Reynolds number defined as $Re = U_\infty L/\nu$; pressure is normalized with $Re^{-1}\rho U_\infty^2$, ρ being the density. Notice that, because of the scaling, Re does not appear in the equations, i.e. the present approach is Reynolds-number independent (Luchini 2000). More specifically, all results presented in the following sections are valid for any (large enough) Reynolds number, the only difference being in the scaling of the relevant dimensionless quantities, and in particular of the amplification which is always proportional to the Reynolds number itself.

System (2.1) requires six boundary conditions, three at the wall, $y = 0$, and three for $y \to \infty$:

$$
\left.
\begin{aligned}
u &= 0 && \text{at} \quad y = 0, & u &= 1 && \text{for} \quad y \to \infty, \\
v &= v_w && \text{at} \quad y = 0, & w &= 0 && \text{for} \quad y \to \infty, \\
w &= 0 && \text{at} \quad y = 0, & p &= 0 && \text{for} \quad y \to \infty,
\end{aligned}
\right\}
\tag{2.2}
$$

where $v_w(x, z)$ is the wall-normal velocity component due to blowing or suction at the wall (zero if no control is applied). System (2.1) is parabolic in x and therefore initial conditions are required. However, only two initial conditions are allowed, as discussed in Luchini & Bottaro (1998). When the streamwise component u is uniformly equal to 1 upstream of the leading edge, the constraint relating the initial conditions for v and w to each other simply reduces to the continuity equation. The initial conditions therefore are

$$
\left.
\begin{aligned}
u(0, y, z) &= 1, \\
v(0, y, z) &= v_0(y, z),
\end{aligned}
\right\}
\tag{2.3}
$$

where $v_0(y, z)$ represents the initial free-stream perturbation and $w(0, y, z) = w_0(y, z)$ can be retrieved from the equation

$$
\frac{\partial v_0(y, z)}{\partial y} + \frac{\partial w_0(y, z)}{\partial z} = 0.
$$

2.1. Choice of the objective function and initial conditions

In previous work concerning the linear algebraic instability and its optimal control, the perturbation kinetic energy was always taken as a measure of the level of perturbations, even if this is not necessarily the only physical quantity signalling the beginning of transition. Here, we adopt as objective function

$$
\mathscr{J} = \alpha_1 E_{out} + \alpha_2 E_{mean},
\tag{2.4}
$$

and work on the assumption that the initial energy E_{in} is fixed at the value E_0. Here, E_{out} is the disturbance energy at the end of the plate and E_{mean} the integral of the energy over the whole length. The coefficients α_1 and α_2 are used to weight the relative importance of the two energies in the cost function. A cost based on the mean energy seems to be more effective when dealing with optimal control problems. As shown by Cathalifaud & Luchini (2000), optimal control based on minimizing the final energy E_{out} alone can produce a very large transient energy amplification before the final streamwise position, with possible undesired consequences on boundary-layer transition. In most of the cases considered here, $\alpha_1 = 0$ and $\alpha_2 = 1$ will be assumed.

We remark that the gain G, because of the chosen scaling, takes the general form

$$G = \frac{\alpha_1 E_{out} + \alpha_2 E_{mean}}{E_{in}} = Re \frac{\alpha_1 E_u|_{x=1} + \alpha_2 \int_0^1 E_u \, dx}{\left[\frac{1}{2Z} \int_{-Z}^{Z} \int_0^\infty (|v_0|^2 + |w_0|^2) \, dy \, dz \right]_{x=0}} \quad (2.5)$$

with

$$E_u(x) = \frac{1}{2Z} \int_{-Z}^{Z} \int_0^\infty |u'|^2 \, dy \, dz.$$

The disturbance u', which is the deviation of the streamwise velocity component from its mean, is set to zero at $x = 0$ because, owing to its different scaling with respect to the v and w components, this choice guarantees the maximal gain in the large-Reynolds-number limit. As a consequence, Re acts as a multiplicative parameter for the gain, and all the numbers that will be read in figure 2 and the following ones must eventually be multiplied by the actual Reynolds number of the flow (typically of the order of 10^6). The local energy of the streaks $E_u(x)$ contains only the streamwise velocity component because retaining the term $Re^{-1}(|v'|^2 + |w'|^2)$ would be inconsistent with the inner–outer expansion from which the boundary-layer approximation is derived (Luchini 2000).

2.2. *Constrained optimization and linear adjoint problem*

Once the objective function to be minimized has been chosen, the next step is to devise an optimization technique able to determine the boundary condition at the wall that renders the objective function minimal for a given initial condition $v_0(y, z)$ and for a given cost of the control, which we assume to be measured by the control energy

$$E_w = \left[\int_0^1 |v_w|^2 \, dx \right]_{y=0}. \quad (2.6)$$

There are classically two ways to do this: one is to incorporate the cost of the control in the total cost function with a suitable penalty factor taking account of the different physical meaning of the perturbation energy (aptitude to induce transition) and control energy (external work necessary to produce it); the second is to impose a given value E_{w0} of the control energy as a constraint, in the form

$$E_w(v_w) = E_{w0} \quad (2.7)$$

and to perform a constrained optimization.

Practically, in both cases a parametric study must be performed, because the relative weight of perturbation and control energy may vary from case to case. In a parametric study, the two approaches are completely equivalent, because at the

point where control energy is the same they yield the same result. The second choice, however, allows us to parameterize our curves with direct reference to the control energy, and therefore to obtain an easier graphical representation of the results.

When robust control is considered, both the initial perturbation and the vertical velocity at the wall are to be simultaneously optimized. In this case, the initial condition $v_0(y, z)$ is an additional unknown that satisfies the constraint:

$$E_{in}(v_0) = \left[\frac{1}{2Z} \int_{-Z}^{Z} \int_0^\infty (|v_0|^2 + |w_0|^2) \, \mathrm{d}y \, \mathrm{d}z \right]_{x=0} = E_0. \qquad (2.8)$$

Since, at $x = 0$, w_0 is uniquely determined by v_0, the initial perturbation energy is written as a function of v_0 only.

The optimization technique is conceptually just an extension of the method used in Zuccher *et al.* (2004) to find optimal perturbations, although some additional care is needed in the case of robust control because the target is a saddle point in parameter space. We first introduce the functional

$$\mathscr{L} = \mathscr{J} + \frac{1}{2Z} \int_{-Z}^{Z} \int_0^\infty \int_0^1 a[u_x + v_y + w_z] \, \mathrm{d}x \, \mathrm{d}y \, \mathrm{d}z$$

$$+ \frac{1}{2Z} \int_{-Z}^{Z} \int_0^\infty \int_0^1 b[(uu)_x + (uv)_y + (uw)_z - u_{yy} - u_{zz}] \, \mathrm{d}x \, \mathrm{d}y \, \mathrm{d}z$$

$$+ \frac{1}{2Z} \int_{-Z}^{Z} \int_0^\infty \int_0^1 c[(uv)_x + (vv)_y + (vw)_z + p_y - v_{yy} - v_{zz}] \, \mathrm{d}x \, \mathrm{d}y \, \mathrm{d}z$$

$$+ \frac{1}{2Z} \int_{-Z}^{Z} \int_0^\infty \int_0^1 d[(uw)_x + (vw)_y + (ww)_z + p_z - w_{yy} - w_{zz}] \, \mathrm{d}x \, \mathrm{d}y \, \mathrm{d}z$$

$$+ \lambda_0[E_{in}(v_0) - E_0] + \lambda_w[E_w(v_w) - E_{w0}], \qquad (2.9)$$

where $a(x, y, z)$, $b(x, y, z)$, $c(x, y, z)$, $d(x, y, z)$, λ_0 and λ_w are Lagrange multipliers, and then impose that $\delta\mathscr{L} = 0$ at a point of minimum or at a saddle point for $\mathscr{J}$, i.e. that the Fréchet derivative of $\mathscr{L}$ with respect to all dependent variables must vanish. In so doing, it is easy to see that all direct equations are recovered, and that a set of linear, adjoint equations appear; they read

$$c_y + d_z = 0, \qquad (2.10a)$$

$$a_x + 2b_x u + b_y v + b_z w + c_z v + d_x v + d_x w + b_{yy} + b_{zz} = \alpha_2 u, \qquad (2.10b)$$

$$a_y + b_y u + c_x u + 2c_y v + d_y w + c_z w + c_{yy} + c_{zz} = 0, \qquad (2.10c)$$

$$a_z + b_z u + c_z v + d_y v + d_x u + 2d_z w + d_{yy} + d_{zz} = 0. \qquad (2.10d)$$

This system is backward parabolic and therefore it needs initial conditions at $x = 1$, as well as boundary conditions at the wall and in the free stream. All the necessary conditions can be obtained in the process of integration by parts that has led to (2.10). The boundary conditions are

$$\left. \begin{array}{lllll} b = 0 & \text{at} \ y = 0, & & b = 0 & \text{for} \ y \to \infty, \\ c = 0 & \text{at} \ y = 0, & a + 2cv + c_y = 0 & \text{for} \ y \to \infty, \\ d = 0 & \text{at} \ y = 0, & & d = 0 & \text{for} \ y \to \infty, \end{array} \right\} \qquad (2.11)$$

and the initial conditions read

$$
\left.\begin{aligned}
a + 2ub + \alpha_1 \frac{\mathscr{D}E_{out}}{\mathscr{D}u} &= 0 \quad \text{at} \quad x = 1, \\
c = d &= 0 \qquad\qquad \text{at} \quad x = 1,
\end{aligned}\right\} \tag{2.12}
$$

where the latter two are not independent because of (2.10*a*) and $\mathscr{D}E_{out}/\mathscr{D}u$ is the Fréchet derivative of the final energy with respect to a variation in the streamwise velocity component.

Finally, the optimality conditions at $x = 0$ and $y = 0$, which relate the direct to the adjoint problem, reduce to

$$
\left.\begin{aligned}
c - \int d_y \, \mathrm{d}z - \lambda_0 \frac{\mathscr{D}E_{in}}{\mathscr{D}v_0} &= 0 \quad \text{at} \quad x = 0, \\
a + c_y - \lambda_w \frac{\mathscr{D}E_w}{\mathscr{D}v_w} &= 0 \qquad \text{at} \quad y = 0.
\end{aligned}\right\} \tag{2.13}
$$

The direct and adjoint equations are discretized by a mixed spectral–finite difference approach described and validated in Zuccher *et al.* (2004).

2.3. *Iterative optimization*

The iterative technique employed to drive $\delta\mathscr{L}$ to zero is summarized here. It corresponds to the procedure outlined by Bewley *et al.* (2000).

1. An initial guess is chosen for the initial condition v_0 at $x = 0$ and boundary condition, v_w at $y = 0$.

2. The parabolic direct problem (2.1) is numerically solved by marching forward in space from $x = 0$ to $x = 1$.

3. At $x = 1$, the objective function $\mathscr{J}$ is evaluated and the initial condition for $a^* = a + 2ub$ is obtained from the relationship

$$
a^* = -\alpha_1 \frac{\mathscr{D}E_{out}}{\mathscr{D}u}.
$$

If the objective is the integral of the energy over the whole domain (i.e. if $\alpha_1 = 0$), the condition is obviously $a^* = 0$.

4. The adjoint problem (2.10) is numerically solved together with the initial conditions (2.12) and boundary conditions (2.11), by marching backward in space from $x = 1$ to $x = 0$.

5. Once the adjoint solution is known, the optimality conditions (2.13) are used to obtain the next best guess of initial and boundary conditions, with a Lagrange multiplier chosen to satisfy the relevant constraint, and the procedure can restart from step 2. The loop stops whenever the difference in $\mathscr{J}$ between two consecutive iterations becomes smaller than a prefixed threshold.

In the optimal perturbation or optimal control problem, only one of the conditions (2.13) is updated, whereas in robust control, each condition is updated in turn, performing a few iterations on each. In robust control, the optimal perturbation is first computed for a fixed boundary condition. Steps 2 to 5 are carried out using the updated initial condition and, if the gain is lower than that of the previous step, the relaxation factor of the gradient algorithm is halved (this technique is described in Zuccher *et al.* 2004). The step is repeated until a larger gain is found. After having updated the initial condition for a fixed control, the cycle of steps from 2 to 5 is repeated varying the control. The new control is also computed via a gradient iteration of variable step size meant to satisfy the second of the optimality conditions (2.13).

The relaxation parameter is halved and the procedure repeated whenever the gain at iteration $(i + 1)$ exceeds that obtained at iteration (i).

2.4. *Optimal control and robust control*

The search for the optimal control proceeds very similarly to the search for the optimal perturbation, with the obvious change that the objective function is to be minimized rather than maximized. In the more general case of robust control, on the other hand, the required extremum is a saddle point corresponding to an initial condition which maximizes the gain and a boundary condition at the wall which minimizes the gain.

A fully general dependence of the initial optimal perturbation on the spanwise coordinate z is assumed and the variables are expanded in a Fourier series in z, in the domain $-\pi/\beta \leqslant z \leqslant \pi/\beta$, with β the spanwise wavenumber. The Fourier coefficients characterizing the initial conditions are:

$$
\left.
\begin{array}{ll}
\text{mode } n = 0 & \text{mode } n \geqslant 1 \\[6pt]
U_0(0, y) = 1, & U_n(0, y) = 0, \\
V_0(0, y) = 0, & V_n(0, y) = V_n^0(y), \\
W_0(0, y) = 0, & W_n(0, y) = W_n^0(y),
\end{array}
\right\}
\tag{2.14}
$$

with V_n^0 and W_n^0 related to each other by the continuity equation.

The control, on the other hand, for the reasons expounded in §1, is chosen to be constant in the spanwise direction, so as to represent a uniform suction/blowing (it will actually turn out to be suction) applied at the wall without any knowledge of the amplitude or phase of the oncoming disturbances. Therefore, the boundary condition at $y = 0$ is different from zero for the wall–normal component of mode zero only:

$$
\left.
\begin{array}{ll}
\text{mode } n = 0 & \text{mode } n > 0 \\[6pt]
U_0(x, 0) = 0, & U_n(x, 0) = 0, \\
V_0(x, 0) = v_w(x), & V_n(x, 0) = 0, \\
W_0(x, 0) = 0, & W_n(x, 0) = 0.
\end{array}
\right\}
\tag{2.15}
$$

Functions $V_n(0, y)$ and $V_0(x, 0)$ are, respectively, the optimal perturbation and the optimal control to be determined.

3. Optimal control: parametric study

3.1. *Different objective functions – linear case*

Our first result concerns the different controls generated by the two objective functions $\mathscr{J} = E_{out}$ and $\mathscr{J} = E_{mean}$. Results are shown in figure 1 for a very low initial energy, $E_0 = 10^{-7}$, where the behaviour is still linear, and for a reasonably large control energy $E_w = 1$. For each case, the optimal wavenumber computed by Zuccher *et al.* (2004) has been chosen, i.e. $\beta = 0.45$ for $\mathscr{J} = E_{out}$ and $\beta = 0.547$ for $\mathscr{J} = E_{mean}$. The initial optimal perturbations for these tests are those obtained in the absence of control. If the objective function is the final energy, nothing prevents the energy from being larger at an intermediate x than at the final station. This actually happens, although to a small degree here, as shown in figure 1(*a*). Therefore, the choice of the final energy as the objective to be minimized, just as pointed out (for a different type of control) by Cathalifaud & Luchini (2000), produces a non-monotonic increase of the energy that is liable to lead to transition even before the end of the boundary-layer
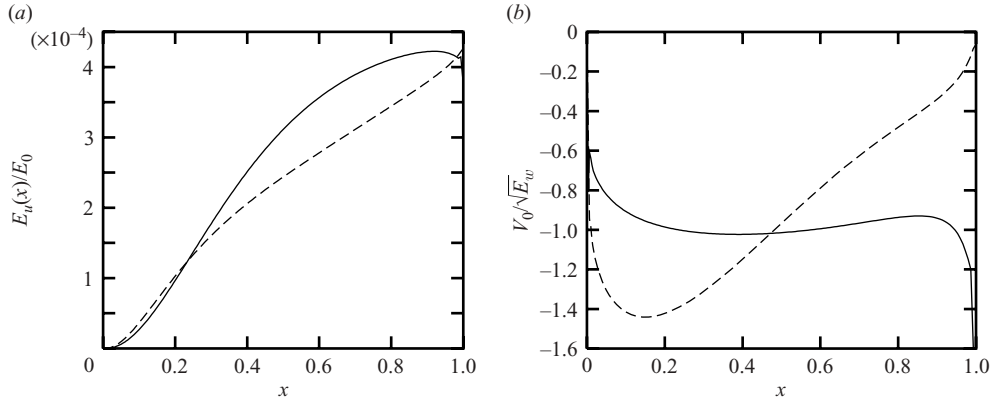
FIGURE 1. Optimal control: comparison between two different objective functions, linear behaviour. $E_0 = 10^{-7}$, $E_w = 1$, $\beta = 0.45$ for ——, $\mathscr{J} = E_{out}$, $\beta = 0.547$ for - - -, $\mathscr{J} = E_{mean}$. (*a*) Disturbance energy, normalized by E_0, as a function of x. (*b*) Optimal suction at the wall normalized with $\sqrt{E_w}$.

region considered. On the other hand, if the objective function is $\mathscr{J} = E_{mean}$, i.e. the integral of the energy over the whole domain, the energy curve grows monotonically, as shown in figure 1(*a*). At the cost of a slightly higher energy at $x = 1$, the energy remains considerably lower than in the previous case over most of the domain.

From these somewhat empirical considerations (and on the basis of the analogous results obtained in different contexts by Cathalifaud & Luchini 2000 and Corbett & Bottaro 2001) it is clear that if the purpose is to control the energy growth, it is preferable to minimize the mean energy rather than the energy at the final station. For this reason, in the following tests, we consider the objective function $\mathscr{J} = E_{mean}$, and the corresponding gain is noted G_{mean}. The same strategy was adopted for the control of infinitesimal disturbances by Pralits *et al.* (2002) and, for the case of streaks, their computed control law (see their figure 4*a*) is quite similar to ours. Incidentally, we note that the control distributions computed (figure 1*b*) are rather smooth, with the possible exception of the leading and the trailing edge of the plate. The issue of the smoothness of the control law (which bears also on the parabolic nature of the governing equations) could be addressed by penalizing, for example, the gradient of the control in the cost functional. This strategy has been adopted by Airiau *et al.* (2003), but eventually it proved to be unnecessary. In fact, they also compared their unpenalized results based on Prandtl's equations to full Navier–Stokes calculations, under the same control distributions, and concluded that shortly downstream of the region where sharp peaks of the control velocity appeared, the two solutions coincided and that, even in extreme cases, 'the prediction from the parabolic model' (in the absence of penalization on $\partial v_w / \partial x$) 'met the criteria of quality and accuracy required by the present application.'

Different ways to analyse the data can be devised; we have chosen two initial energy values, one close to the linear regime, $E_0 = 1$, and one in the nonlinear regime, $E_0 = 500$, and for both of them we shall now change the other parameters, one at a time.

3.2. *Comparison for varying β and E_w*

In figure 2, the mean gain is reported for $E_0 = 1$ and $E_0 = 500$ as a function of the spanwise wavenumber β and for different values of the control energy at the wall E_w.
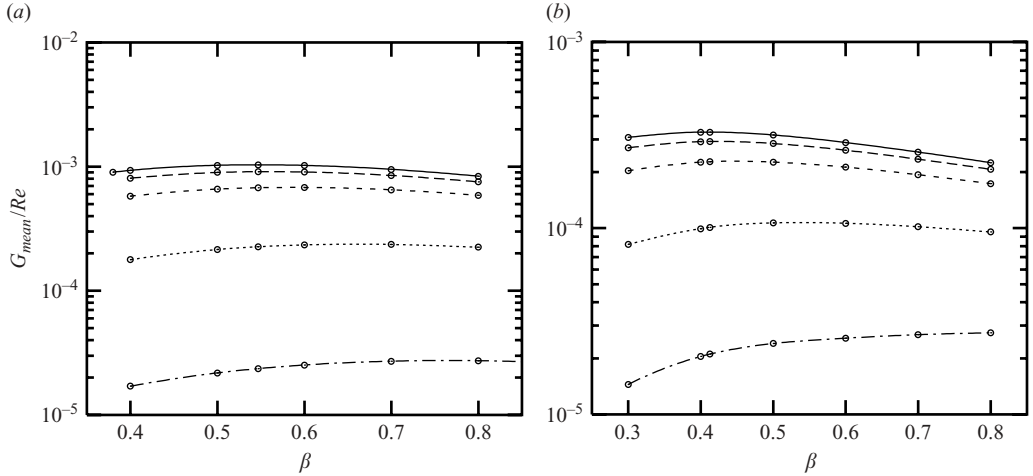
(*a*)

(*b*)

FIGURE 2. Curve of the gain as a function of the spanwise wavenumber β for different values of the control energy at the wall E_w. (*a*) Initial energy $E_0 = 1$. (*b*) Initial energy $E_0 = 500$. ———, uncontrolled; − − −, $E_w = 0.01$; - - -, 0.1; ·····, 1.0; —·—, 5.0.

The solid lines in figures 2(*a*) and 2(*b*) represent the uncontrolled case. In the case of low initial energy (figure 2*a*), it can be seen that a control energy $E_w = 0.01$ produces a barely visible difference from the uncontrolled case ($E_w = 0$), as we should expect. The maximum of the curve is still very close to $\beta = 0.547$, the optimal β for $E_w = 0$, and the gain is just slightly lower, because of the control.

If the control energy at the wall is increased, $E_w = 0.1$, the position of the maximum shifts towards a higher wavenumber β, and the difference with the uncontrolled case becomes more evident. The same trend also characterizes the case $E_w = 1.0$ and $E_w = 5.0$. For the highest control $E_w = 5.0$, the position of the maximum is located at $\beta = 0.767$, which is 40% larger than the optimal wavenumber without control. For a higher initial energy, $E_0 = 500$, the same general dependence on the control energy E_w is found: for high control energies the optimal wavenumber monotonically shifts towards higher values (cf. figure 2*b*). For the strongest control employed, $E_w = 5.0$, the maximum of the curve is outside the range considered for these investigations, whereas without control it was at $\beta = 0.413$. It is noticeable that, although nonlinear interactions among all the Fourier modes are fully accounted for in the equations, the damping effect of the control prevails smoothly up to very large control energies without any undesired higher-harmonic excitation.

We shall now let the control energy at the wall vary for a fixed wavenumber β, equal to the value giving the maximum gain without control (§ 3.3), and then fix the control energy E_w and observe the dependence on the wavenumber β (§ 3.4). Lastly, we shall let the energy change while choosing the optimal wavenumber (the wavenumber for which the curve $G_{mean}(\beta)$ reaches its maximum) for each E_w (§ 3.5).

3.3. *Comparison at fixed* β

Here, β is fixed at a reference value equal to the optimal wavenumber of the uncontrolled case, respectively $\beta = 0.547$ for $E_0 = 1$ and $\beta = 0.413$ for $E_0 = 500$. In figure 3, the behaviour of the energy $E_u(x)/E_0$ is displayed for increasing control energy E_w. Even a small control energy at the wall, $E_w = 0.01$, produces a visible effect on the energy growth, and this is true for both initial energies $E_0 = 1$ and $E_0 = 500$. With increasing control effort, the deviation from the uncontrolled case
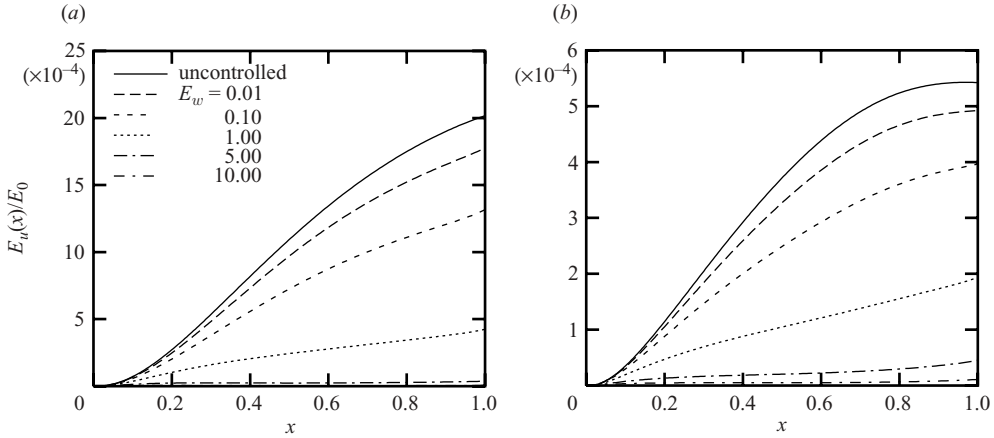
FIGURE 3. Comparison at fixed wavenumber β: perturbation energy $E_u(x)/E_0$ for increasing control energy E_w at the wall. (a) $E_0 = 1$ and $\beta = 0.547$; (b) $E_0 = 500$ and $\beta = 0.413$.
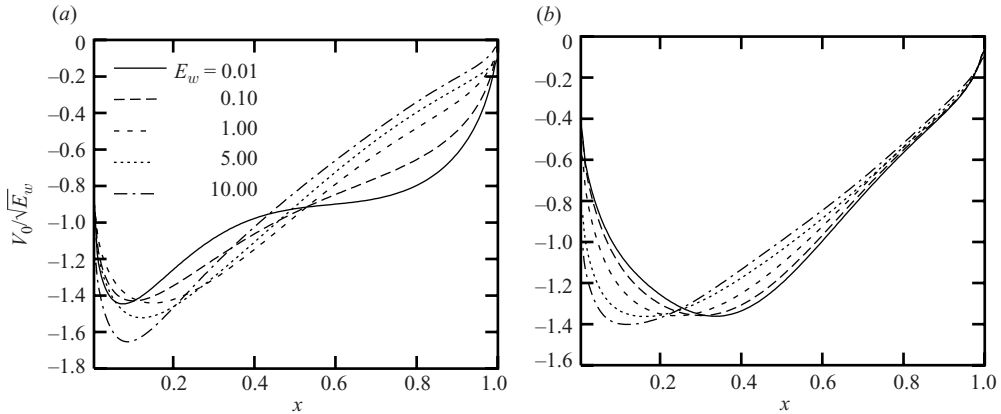

FIGURE 4. Comparison at fixed wavenumber β: optimal suction profile at the wall $V_0/\sqrt{E_w}$ for increasing control energy E_w. (a) $E_0 = 1$ and $\beta = 0.547$; (b) $E_0 = 500$ and $\beta = 0.413$.

becomes more appreciable and for very high control energies, $E_w = 5$ and $E_w = 10$, the reduction in $E_u(x)$ is so strong that the corresponding curve is flattened against the axis in figure 3. In these cases, $E_u(x)/E_0$ is of the order of 10^{-5} for both low and high initial energy E_0.

In figure 4, the optimal suction profiles at the wall are presented for the same cases. Each profile has been normalized with respect to $\sqrt{E_w}$ in order to emphasize the difference in shape arising from different control energies. The first remark is that the control velocity at the wall, whose sign was not *a priori* determined, in fact, turns out to be always negative, so that only suction is applied. For the lower initial energy $E_0 = 1$ (figure 4a), the increasing control effort E_w makes the profile become more regular. The maximum suction, however, is always confined within the first 20% of the total flat-plate length. On the contrary, for the higher initial energy, $E_0 = 500$, the profiles show an increased dependence of the maximum-suction location on the control energy. Moreover, for $E_0 = 500$, the suction velocity features a smoother dependence on x than for $E_0 = 1$. A slight difference is therefore found between the linear and the nonlinear regimes, even though the optimal suction always
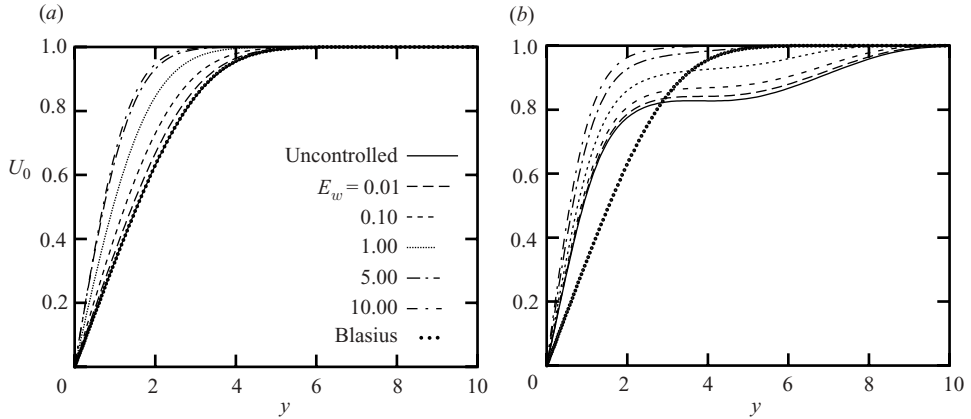
FIGURE 5. Comparison at fixed wavenumber β: streamwise velocity component u of mode zero at $x = 1$ as a function of y for increasing control energy E_w at the wall. (a) $E_0 = 1$ and $\beta = 0.547$; (b) $E_0 = 500$ and $\beta = 0.413$.

peaks next to the leading edge. The reason for this is very likely to be related to the intuitive fact that in order to oppose the growth of a disturbance field, it is better to act in the proximity of the most receptive region. Luchini & Bottaro (1998) actually showed that the wall–receptivity coefficients of the system have their maximum at $x = 0$.

In order to investigate how the mean flow is affected by the control, in figure 5, we plot mode zero at the final station for $E_0 = 1$ and $E_0 = 500$. In agreement with the optimal-perturbation analysis of Zuccher *et al.* (2004), for $E_0 = 1$ in figure 5a, Blasius and uncontrolled profiles practically coincide, showing that nonlinear effects are irrelevant at this energy level. The control at the wall modifies the mean flow in a way that resembles the asymptotic suction or an accelerated Falkner–Skan profile. It should be remarked that, since the profile becomes fuller and its derivative at the wall is increased, stabilization of the flow is obtained at the expense of an increased drag, just as in classical boundary-layer suction. For high initial energy, $E_0 = 500$, the uncontrolled mode zero looks very different from Blasius' because of the strong distortions induced by nonlinear effects. When the control is applied (figure 5b), the ensuing reduction in disturbance amplification carries along a reduction in nonlinear interactions, and we can see that the stronger the control, the closer the profile is to that corresponding to low initial energy. For example, at $E_w = 10$, the profiles for $E_0 = 1$ and $E_0 = 500$ are almost the same.

In order to render more visually apparent how the optimal control attenuates the disturbance induced by the optimal perturbation, figure 6 displays the crossflow velocity (v, w) vectors and figure 7 the iso-streamwise-velocity (u) contours in the (z, y)-plane at the outlet station $x = 1$, where the difference between the uncontrolled and controlled cases is greatest, for large initial energy $E_0 = 500$ and the corresponding optimal $\beta = 0.413$. Without any control ($E_w = 0$, figure 6a), the optimal perturbation induces streamwise vortices which drift away from the wall with increasing x. At $x = 1$, the centres of these vortices are spaced by half a wavelength in the spanwise direction, and located close to the boundary-layer edge ($y \approx 4$). When the control is applied ($E_w = 10$, figure 6b), a reduction of both vortex size and intensity leads to a flow field which is quite regular and strongly different from the uncontrolled case. A completely uniform flow can be obtained at $x = 1$ for the same control energy when
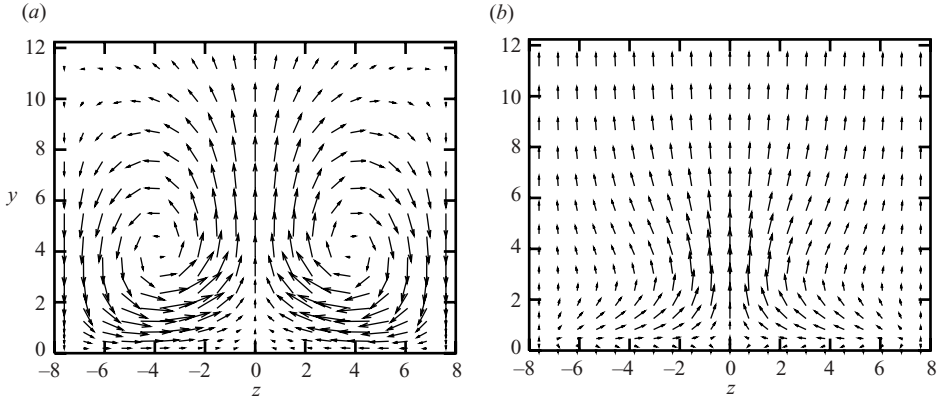
FIGURE 6. $E_0 = 500$, $\beta = 0.413$. Velocity vectors (v, w) in the (z, y)-plane at $x = 1$. In both figures, the vectors are scaled in the same manner. (*a*) Uncontrolled. (*b*) $E_w = 10$.
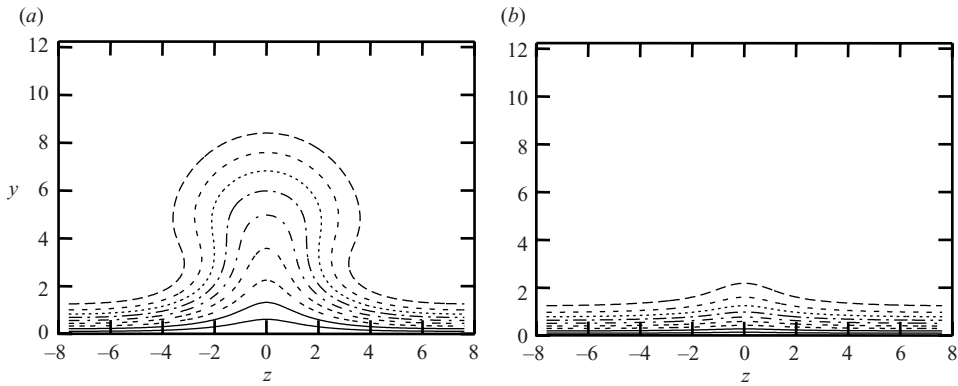

FIGURE 7. $E_0 = 500$, $\beta = 0.413$. Streamwise velocity u isolines in the (z, y)-plane at $x = 1$. (*a*) Uncontrolled. (*b*) $E_w = 10$.

$E_0 = 1$. The main physical effect of the control is therefore to flatten the vortices against the wall.

The contours of the streamwise velocity u, reported in figure 7, confirm the above interpretation. For an unperturbed Blasius profile, the contour plot would be made of lines parallel to the z-axis; therefore the deviation from such a behaviour can visibly suggest how strong the disturbance is. Without any control (figure 7*a*), the strong lift-up induced by the optimal perturbation is responsible for the typical 'mushroom' shape observed (cf. also the nonlinear, sub-optimal streak computed by Andersson *et al.* 2001). When the control is applied and the disturbance thus reduced, two effects are visible on the plots. The first is that the contour lines become almost parallel to the z-axis, the second is a reduction in both the horizontal and vertical extent of the perturbed region. We can see that without control the contour lines are very bulged and the region where this happens is located approximately between $z = -4$ and $z = 4$; with control ($E_w = 10$), the bulge decreases in amplitude and at the same time in extent, becoming confined between $z = -2$ and $z = 2$.

The plots shown in figure 7 visually confirm that the main effect of wall suction is to bring the disturbance closer to the wall. A perhaps less obvious conclusion is that
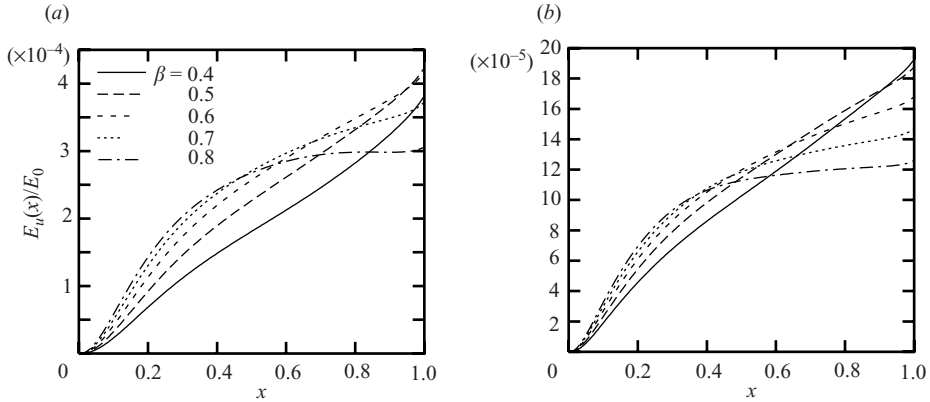
FIGURE 8. Comparison at fixed control energy $E_w = 1$ for increasing wavenumbers β: perturbation energy $E_u(x)/E_0$. (a) $E_0 = 1$; (b) $E_0 = 500$.
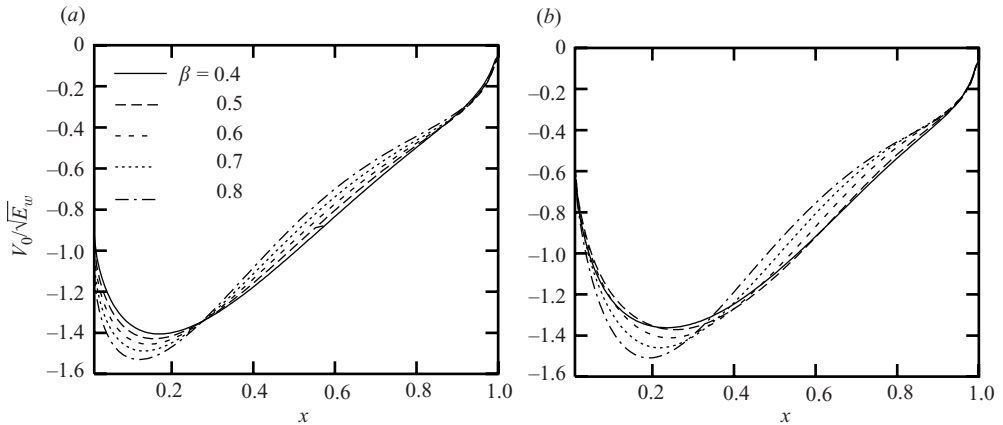

FIGURE 9. Comparison at fixed control energy $E_w = 1$ for increasing wavenumbers β: optimal suction profile at the wall $V_0/\sqrt{E_w}$. (a) $E_0 = 1$; (b) $E_0 = 500$.

at the same time it confines the perturbation horizontally to a smaller neighbourhood of the lift-up point.

3.4. *Comparison at fixed E_w*

Another way to extract information from our data is to consider how the results change as a function of the wavenumber β, for a fixed control energy E_w. In figure 8, the streamwise evolution of the perturbation energy $E_u(x)/E_0$ is reported for $E_w = 1$ and several wavenumbers (for each of the two initial energies $E_0 = 1$ and $E_0 = 500$). Plots are normalized with the corresponding E_0, in order to make it possible to compare the results in terms of gain. One can easily see that there is no big difference between low– and high–initial–energy profiles when looked at in this way. For both initial energies, when the wavenumber is large the energy profile develops the typical plateau already identified by Zuccher *et al.* (2004).

In figure 9, the optimal suction profiles at the wall are reported for $E_w = 1$. The main significant difference between low and high E_0 is in the position of the maximum control, which is closer to the leading edge for $E_0 = 1$. The general trend of a larger suction applied near the leading edge is, however, confirmed. The maximum suction
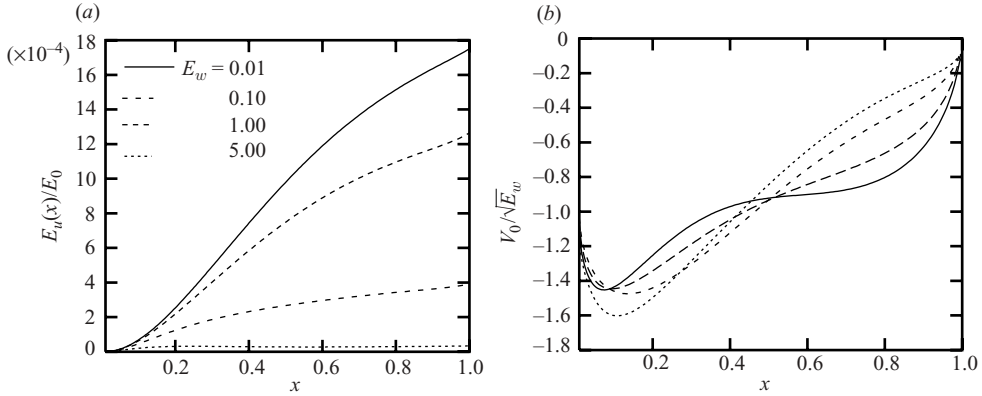
FIGURE 10. Comparison at optimal wavenumber β and $E_0 = 1$ for different values of the control energy E_w. (a) perturbation energy $E_u(x)/E_0$; (b) optimal suction profile at the wall $V_0/\sqrt{E_w}$.

increases in absolute value and its position moves towards the leading edge as the wavenumber increases.

3.5. *Comparison at the optimal β*

The last data comparison we present is obtained by changing the wavenumber so as to keep it at the optimal value at the same time as we change the control energy. This is useful to ascertain that a control optimized for a fixed wavenumber does not worsen the instability at a different one. As far as the streamwise energy growth is concerned, (figure 10a) obviously, when the control energy is higher, the whole curve is driven down. On the other hand, the optimal suction profile at the wall shows, at least for $E_0 = 1$, a certain sensitivity to the control energy E_w. The overall trend is quite similar to that observed when the profiles were compared at fixed wavenumber. For this reason, only results regarding $E_0 = 1$ are here reported at the optimal β.

3.6. *Controlling on a finite window*

In all cases considered in the previous sections, the control has always been applied over the whole length of the wall from leading to trailing edge. However, in practical applications to aircraft this solution might be unfeasible, because of the installation of other devices at the leading or trailing edge. For this reason, it is worth checking what happens if the control is applied only on a limited window, in the range $x_1 < x < x_2$ where $x_1 \neq 0$ and $x_2 \neq 1$. This can be obtained easily by penalizing the control energy through a hat-shaped window function, or rather, in order to avoid creating a discontinuity in the wall velocity profile, a smoothed-hat weight function $k(x)$, namely

$$
k(x) = \begin{cases} 1 - \left[\sin\left(\pi \dfrac{x - x_1}{x_2 - x_1} - \dfrac{\pi}{2} \right) \right]^{20} & \text{for } x_1 < x < x_2, \\ 0 & \text{for } x < x_1 \text{ and } x > x_2. \end{cases}
$$

In figure 11, results are shown at fixed control energy $E_w = 1$ for $E_0 = 1$ and $\beta = 0.547$. Different configurations are considered for comparison: without control (solid line), with control from $x = 0$ to $x = 1$, and with control over one or two windows. The streamwise growth of the energy normalized with respect to E_0 (figure 11a) produces the expected results that the lowest integral of the energy over the whole domain is achieved when the control is applied from $x = 0$ to $x = 1$. The same holds
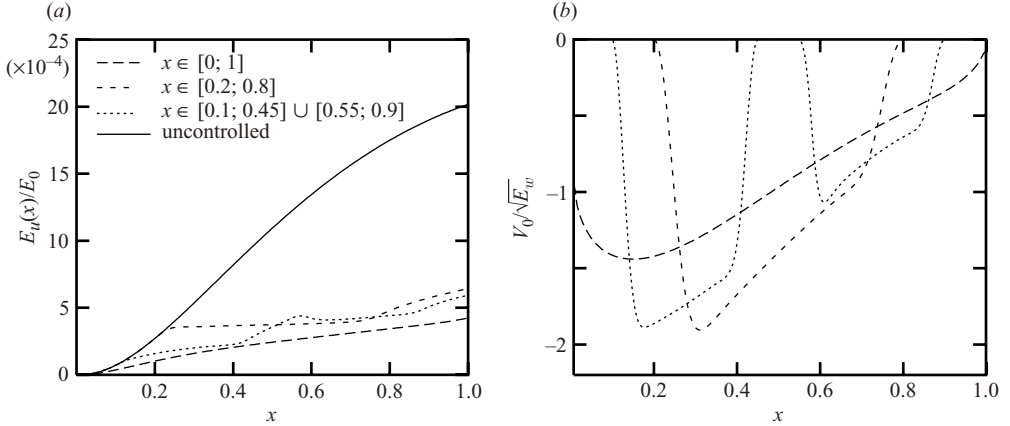
FIGURE 11. Different suction windows at fixed control energy $E_w = 1$ for $E_0 = 1$ and $\beta = 0.547$: (a) perturbation energy $E_u(x)/E_0$; (b) optimal suction profile at the wall $V_0/\sqrt{E_w}$.

true also for the value of the energy at the end of the plate. However, in the windowed cases the overall reduction remains in the same general range.

From the optimal suction profile at the wall (figure 11b), it may also be observed that the strongest control is always applied close to the leading edge, and that when single or multiple windows are employed the profile looks very much like a windowed portion of the original best control. The same trend is observed for large initial energy ($E_0 = 500$), both with and without control windows.

3.7. Skin friction

The most common goal of the laminar-flow-control technique is indirectly to reduce skin friction by increasing the area of a wing surface over which flow is laminar at the expense of the area where flow is turbulent. To reach this objective, we do not usually include skin friction in the cost function, since the effect of a transition delay on skin friction is not directly observable in a stability or optimal-perturbation calculation; as a result of its reduced thickness, however, a controlled boundary layer is likely to be characterized by an increased mean skin friction. It is therefore useful to quantify this increase and verify that it remains small compared to the increase that would be produced by a turbulent flow.

In figure 12, the derivative of U_0 with respect to y at the wall is shown as a measure of the skin friction and compared to the same quantity for a turbulent boundary layer. For this purpose, a Reynolds number has to be chosen, and the turbulent-boundary-layer friction coefficient at that Reynolds number rescaled to the present non-dimensional variables. Since the transition Reynolds number may change with experimental conditions, three (rather conservative) example values are included in the figure. The turbulent friction coefficient has been obtained from Prandtl's low-Reynolds-number correlation for a flat-plate boundary layer (equation 21.12 of Schlichting 1979), namely:

$$\left.\frac{\partial u^*}{\partial y^*}\right|_{y=0} = 0.0296 \frac{U_\infty^2}{\nu} \left(\frac{x U_\infty}{\nu}\right)^{-1/5},$$

where u^* and y^* are dimensional quantities and need to be normalized with respect to U_∞ and δ.

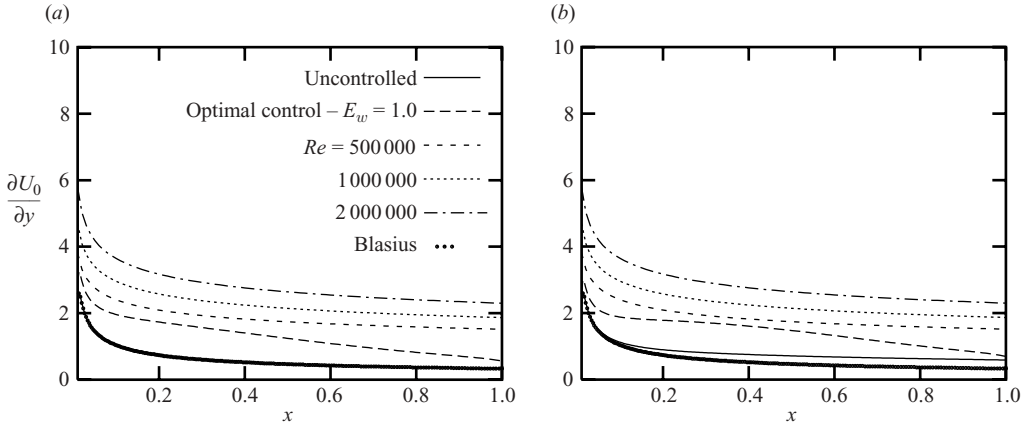FIGURE 12. $\partial U_0/\partial y$ at the wall, in the uncontrolled, controlled ($E_w = 1$) and turbulent boundary layer: (a) $E_0 = 1$ and $\beta = 0.547$; (b) $E_0 = 500$ and $\beta = 0.413$.
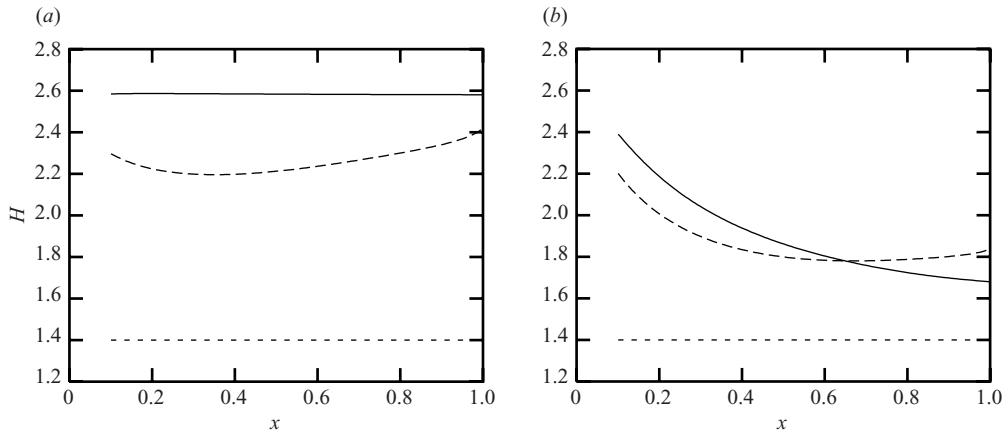

FIGURE 13. Shape factor H, in the uncontrolled (——), controlled ($E_w = 1$) (– – –) and turbulent boundary layer (- - - -): (a) $E_0 = 1$ and $\beta = 0.547$; (b) $E_0 = 500$ and $\beta = 0.413$.

Two cases are reported, for a low initial energy $E_0 = 1$ (figure 12a, at its optimal $\beta = 0.547$) and high initial energy $E_0 = 500$ (figure 12b, at its optimal $\beta = 0.413$). In figure 12a, the initial perturbation is weak, and the uncontrolled velocity profile is essentially Blasius'. The corresponding controlled profile shows a higher wall derivative, and, in fact, qualitatively resembles an accelerating and more stable one. However, when the controlled-flow skin friction is compared to the turbulent skin friction computed for three possible Reynolds numbers (5×10^5, 10^6, 2×10^6), it appears evident that the effect of control on skin friction is, under all circumstances, well below the effect that would be produced by a transition to turbulence.

At high initial energy (figure 12b) the uncontrolled behaviour differs from Blasius' because of the strong nonlinear interactions. In this case too, however, the increased skin friction produced by optimal control is always smaller than any turbulent case considered, confirming the advantage of this optimal-control strategy as an LFC technique. To further illustrate the relative smallness of the mean-flow modification induced by optimal control as opposed to the modification that can be induced by turbulence, figure 13 displays the shape factor H for the uncontrolled, controlled and

turbulent boundary layer. (As a reference for the turbulent case at near-transition Reynolds number, the value $H = 1.4$ has been taken.)

At low initial energy (figure 13*a*) and when no control is applied, the shape factor of the velocity profile does not differ from Blasius' ($H = 2.59$). In the controlled case, H decreases, as can be seen in the figure, to about 2.2, but always remains much higher than 1.4. At high initial energy (figure 13*b*), the uncontrolled shape factor decreases monotonically with x down to less than 1.7. The effect of the control, however, is to restore a higher shape factor, by counteracting in fact the effect of the very strong initial perturbation, leading to values larger than about 1.8. In all cases, the turbulent value of 1.4 is not attained.

4. Robust control: parametric study

In the previous section, the best velocity distribution at the wall was computed so as to minimize the algebraic growth of given initial conditions, chosen to be the optimal perturbations for the uncontrolled flow. However, that calculation did not account for the fact that the optimal perturbations, when the control is on, are possibly different from those that were effective when the control was off. A new question can therefore be asked: what is the initial condition to apply at $x = 0$ in order to generate the maximum energy growth when a suction velocity is applied at the wall, and what is the best control to apply at the wall in order to damp that initial disturbance? This approach, called 'robust control', furnishes both the optimal perturbation and the optimal control at the same time while accounting for each other.

4.1. *Comparison for varying β and E_w*

In figure 14, the gain is reported as a function of the wavenumber for $E_0 = 1$. The solid line represents the optimal-perturbation result, that is to say without any control, the small-dot curves refer to the optimal-control results presented in the previous section and all the other curves are robust control results for different values of E_w. A first remark is that, exactly as in the case of optimal control, an increase in the control energy makes the maximum of the curves shift towards higher wavenumbers, and this shift becomes more pronounced at high E_w. The overall gain curve representing the robust control at each E_w is higher than the corresponding optimal-control curve, as it must be, and the difference increases with E_w. For instance, the curves at $E_w = 5$ feature a gain which in the optimal case is almost half of the corresponding robust one. Clearly, this implies a difference in both optimal control profile at the wall and optimal initial perturbation, when optimal and robust cases are compared.

It should be remarked that the re-increase of the gain at low β observable in some of the curves of figure 14 is a ghost image produced by an aliasing effect, similar to that illustrated in Zuccher *et al.* (2004); namely, the algorithm converges on an optimal solution in which the second harmonic becomes the fundamental, reproducing exactly the same gain and the same physical solution as found in the plot at double the wavenumber.

Energy-growth and suction-profile results will now be presented, first at constant wavenumber and increasing control energy (§4.2), then at fixed control energy E_w and varying wavenumber β (§4.3), and finally at the optimal wavenumber (§4.4).

4.2. *Comparison at fixed β*

Just as for the optimal control, comparisons at fixed β are performed at the wavenumber for which the curve of the gain reaches its maximum in the uncontrolled
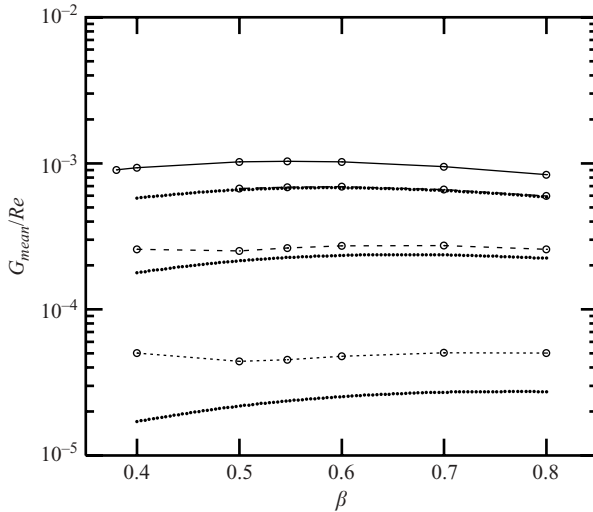
FIGURE 14. Comparison between optimal and robust control for different values of the control energy E_w at $E_0 = 1$. The uppermost curve (thin solid line) is the uncontrolled reference case. The three bold dotted curves represent, from top to bottom, the optimal control cases for $E_w = 0.1$, 1.0 and 5.0 (cf. figure 2). The robust control curves are shown with a dot-dashed line for $E_w = 0.1$ (indistinguishable from the corresponding optimal control curve), a long-dashed line for $E_w = 1.0$ and a short-dashed line for $E_w = 5.0$.
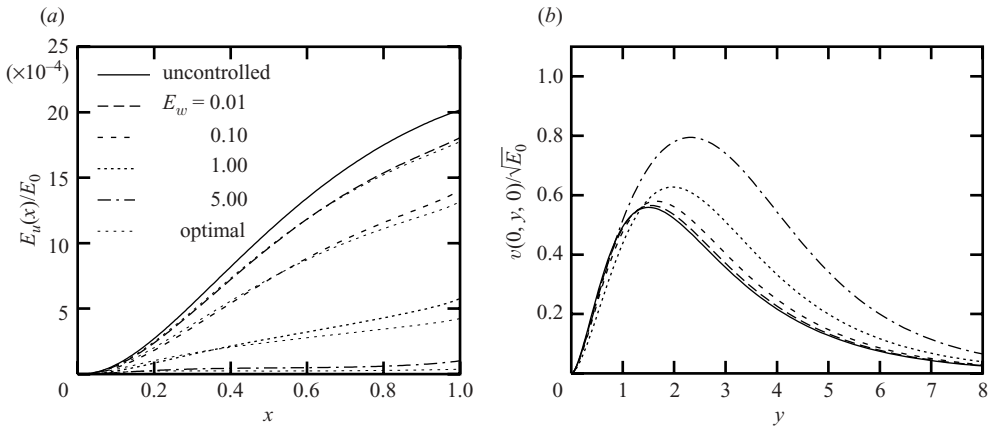

FIGURE 15. Comparison at constant wavenumber $\beta = 0.547$ for increasing control energy E_w at $E_0 = 1$: (a) perturbation energy $E_u(x)/E_0$; (b) optimal perturbation $v_0(y,z)/\sqrt{E_0}$ in the plane $z = 0$.

case. The streamwise energy growth at $\beta = 0.547$ is reported in figure 15 for $E_0 = 1$. The solid line denotes the uncontrolled case; the optimal-control results are also reported for comparison. The mean gain for robust control must obviously be larger than for the optimal case. Nonetheless, the energy curves (figure 15a) of robust control are not everywhere above those corresponding to optimal control. As we would expect, hardly any difference is seen for the lowest control energy $E_w = 0.01$.

In figure 15(b), the optimal perturbation $v_0(y,z)/\sqrt{E_0}$ in the plane $z = 0$ is reported for the same cases as in figure 15(a). The solid line corresponds to the uncontrolled
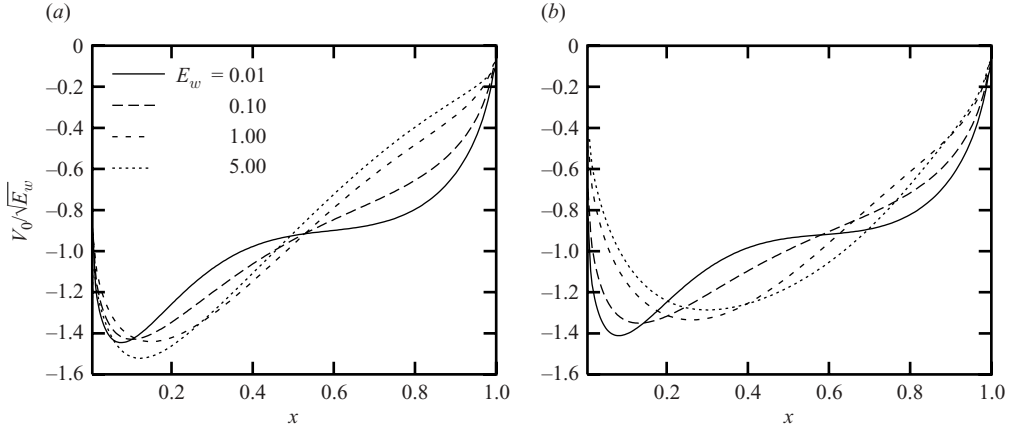
FIGURE 16. Comparison at constant wavenumber $\beta = 0.547$ for increasing control energy E_w. $E_0 = 1$, optimal suction profile at the wall $V_0(x, 0)/\sqrt{E_w}$: (a) optimal control; (b) robust control.
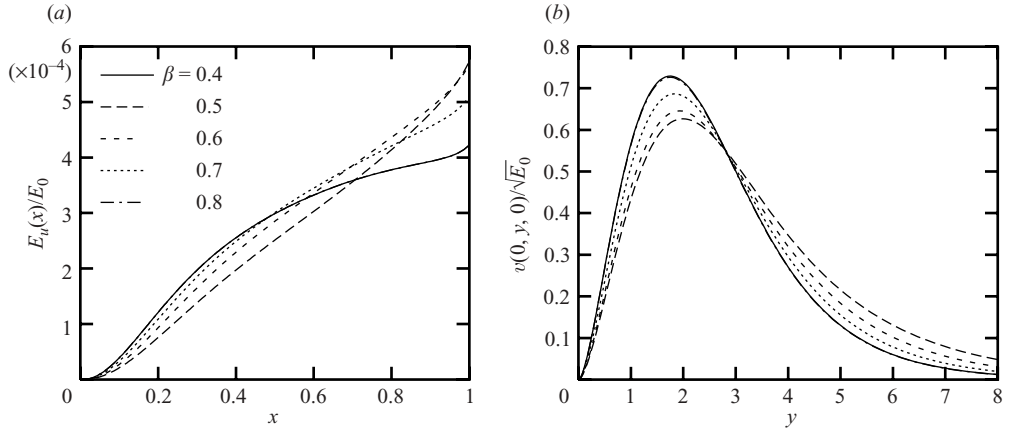

FIGURE 17. Comparison at fixed control energy $E_w = 1$ for increasing wavenumber β, $E_0 = 1$: (a) perturbation energy $E_u(x)/E_0$; (b) optimal perturbation $v_0(y, z)/\sqrt{E_0}$ in the plane $z = 0$.

case, and it can be observed that the optimal-perturbation's maximum gradually shifts outwards with increasing control energy.

In figure 16, the optimal suction profiles are reported for the optimal- and robust-control cases. Figure 16(a) reproduces some of the curves of figure 4(a) for comparison purposes. For control-energy values $E_w > 0.01$, the difference between optimal and robust control becomes visible. It can be observed that the modulus of the control velocity in the robust-control case is always lower than the corresponding optimal-control case, the location where the largest suction needs to be applied is always closer to the leading edge in the optimal-control calculation, and the optimal suction resulting from robust-control computations is more uniform in x.

4.3. Comparison at fixed E_w

Here, the control energy is fixed at $E_w = 1$, and the dependence of the results on the wavenumber β is analysed. In figure 17(a), the streamwise growth of the disturbance energy is reported for $E_0 = 1$. Note that the large-β plateau observed in the
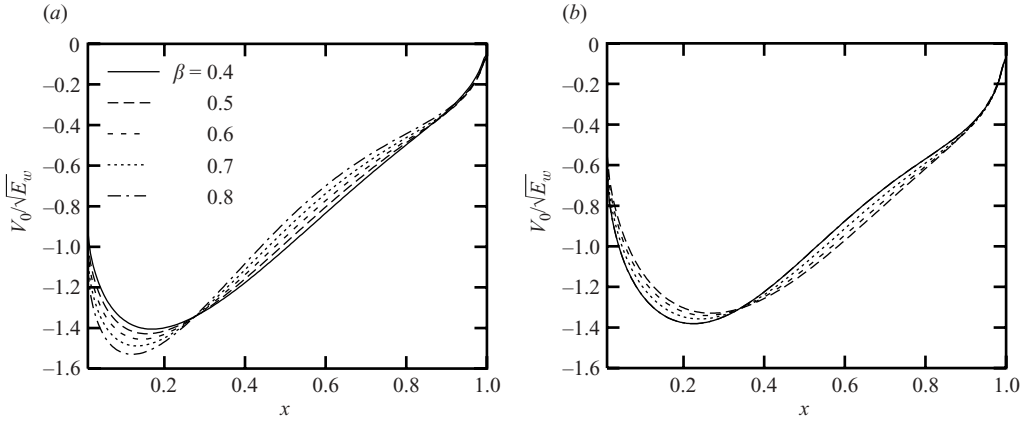
FIGURE 18. Comparison at fixed control energy $E_w = 1$ for increasing wavenumber β. $E_0 = 1$, optimal suction profile at the wall $V_0(x, 0)/\sqrt{E_w}$: (a) optimal control; (b) robust control.

optimal-perturbation results discussed in Zuccher *et al.* (2004), and still present in the optimal-control case (figure 8a), is no longer there. On the contrary, the energy profile grows monotonically with x.

Optimal initial perturbations are displayed in figure 17(b). The position of the maximum of the wall-normal velocity moves towards lower values of y when the wavenumber increases, and the shape of the profile changes smoothly with varying β. For low wavenumbers, $V_1(0, y)$ goes to zero very slowly for $y \to \infty$; on the other hand, for high wavenumbers, the optimal perturbation goes to zero more rapidly as $y \to \infty$. The same features were observed in the absence of control (see Zuccher *et al.* 2004).

It should also be noticed that in figure 17 the flow field obtained for $\beta = 0.4$ is a ghost image of $\beta = 0.8$ with the second harmonic $n = 2$ taking the place of $n = 1$.

In figure 18, optimal wall-suction profiles are plotted for both optimal and robust control. Incidentally, figure 18(b) shows again the same result at $\beta = 0.4$ and $\beta = 0.8$. A remark is that the robust-control results are less dependent on the wavenumber than the optimal ones. This can be quantified by looking at the variation of the suction peak and its location. In the robust-control case, both parameters are within a smaller range and, moreover, the maximum absolute value of the suction velocity is always lower than in the optimal-control case. This general behaviour gives some confidence that the suction profile determined by the robust calculation could be effective in a range of wavenumbers and control energies and not just for the values imposed when it was computed.

4.4. *Comparison at optimal β*

The last comparison is performed while choosing for each control energy the corresponding wavenumber that maximizes the gain. The streamwise evolution of the energy $E_u(x)/E_0$ thus obtained is shown in figure 19(a) for optimal and robust control.

The difference between the two control strategies smoothly increases with E_w without any unexpected change in behaviour up to relatively large values of the control energy (cf. figure 15a). The variation in the optimal initial perturbation calculated in the robust-control framework is reported in figure 19b. With increasing E_w, the position of the maximum moves farther from the wall and the value of the
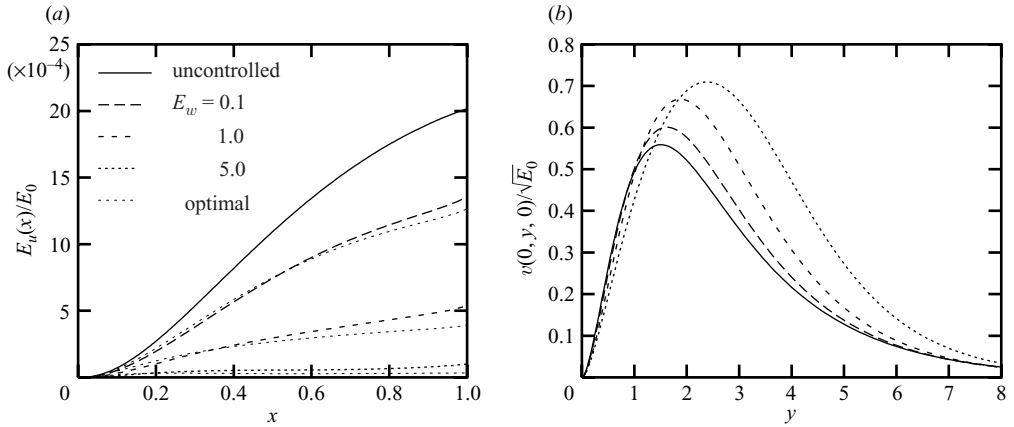
FIGURE 19. Comparison at optimal wavenumber β for increasing E_w and $E_0 = 1$:
(a) perturbation energy $E_u(x)/E_0$; (b) optimal perturbation $v_0(y,z)/\sqrt{E_0}$ in the plane $z = 0$.
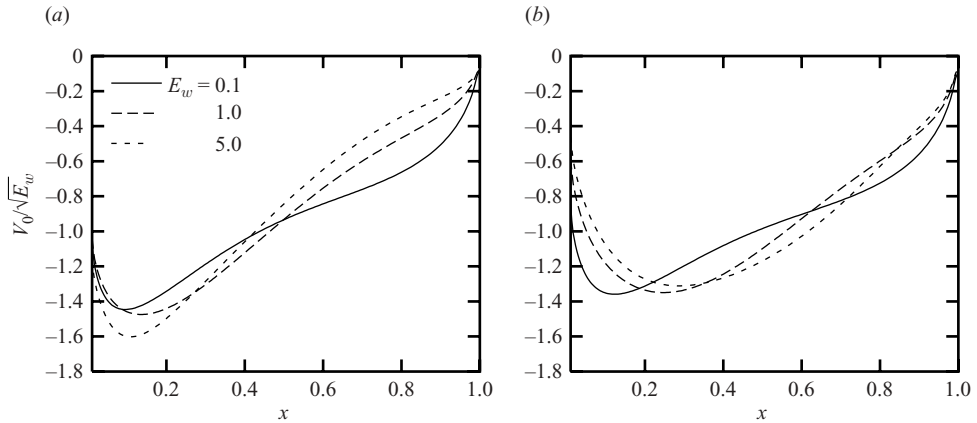

FIGURE 20. Comparison at optimal wavenumber β for increasing E_w. $E_0 = 1$, optimal suction
profile at the wall $V_0(x,0)/\sqrt{E_w}$: (a) optimal control; (b) robust control.

maximum increases at the same time. However, contrary to what happens when the wavenumber is not optimized, all the profiles tend to zero in the same way as $y \to \infty$.

In figure 20, the optimal suction profile $V_0(x,0)/\sqrt{E_w}$ is reported for different values of the control energy, at the optimal wavenumber, comparing optimal- and robust-control results. The wall suction resulting from robust control (figure 20b) turns out to be less sensitive to E_w than the one from optimal control; it is also more regular, with smaller peak values and a maximum located farther downstream than in the optimal-control case.

5. A further remark on the differences between optimal and robust control

In order to synthesize the differences between optimal and robust strategies, in table 1 the optimal wavenumber β_{opt} and corresponding gain G are reported for each control energy E_w in the two cases.

E_w	Robust control β_{opt}	Optimal control β_{opt}	Robust control G/Re	Optimal control G/Re
0.1	0.585	0.588	6.918×10^{-4}	6.801×10^{-4}
1.0	0.655	0.660	2.749×10^{-4}	2.370×10^{-4}
5.0	0.732	0.767	5.062×10^{-5}	2.745×10^{-5}

TABLE 1. Values of optimal wavenumber β and gain G for optimal and robust control as a function of the control energy E_w.

Case	Initial condition at $x = 1$	Boundary condition at $y = 0$	G/Re
OO	Optimal perturbation	Optimal control	2.74×10^{-5}
OR	Optimal perturbation	Robust control	3.67×10^{-5}
RR	Robust perturbation	Robust control	5.02×10^{-5}
RO	Robust perturbation	Optimal control	6.38×10^{-5}

TABLE 2. Values of the mean gain G for different initial perturbations and suction velocities at the wall. $E_0 = 1$, $E_w = 5$ and $\beta = 0.8$.

As observed from the preceding figures, the robust-control suction profile is usually more uniform in x (see figure 20), is quite insensitive to variations of E_w or β, and presents a lower peak at a location which is farther downstream. This results in a sensible difference in the optimal gain G, as reported in table 1 at $E_w = 1$. The optimal wavenumber β_{opt}, on the other hand, does not change much. For the highest control energy $E_w = 5$, for instance, even if the optimal wavenumber decreases only by 5%, the difference in the optimal gain between the robust and optimal case is 84%.

Going a little deeper in the comparison, we could wonder how effective/ineffective the robust control could be when applied to the optimal initial perturbation computed in Zuccher *et al.* (2004), or how (in)effective the optimal control could be when applied to the robust initial perturbation. The possible combinations and the corresponding values of the mean gain, ordered by increasing G, are reported in table 2, for $E_0 = 1$, $E_w = 5$ and $\beta = 0.8$.

The smallest energy gain is found for the optimal-initial-perturbation–optimal-control case, as expected. In fact, the optimal control at the wall computed for a given initial condition is the one that minimizes the objective function among all the possible controls. If, for the same initial optimal perturbation, the robust control (obviously referring to the same E_0, E_w and β) is applied, case OR, a degradation of the control efficiency follows and the gain increases by 23%. Figure 21 shows how this happens. In case OR, the energy, close to the leading edge, grows much faster than in case OO. As stressed before, the reason for this behaviour probably lies in the fact that the robust-control suction always reaches its peak farther downstream than the optimal-control case and therefore is less effective close to the leading edge.

The robust-initial-perturbation–robust-control case (RR) furnishes, by definition, the most disrupting initial condition together with its best control at the wall. For this reason, the gain is higher than in the preceding two cases. However, when the optimal control at the wall is applied to the robust initial condition (case RO), gain becomes even larger (by 27%). It goes without saying that in the presence of a random mixture of all possible perturbations robust control guarantees the best value of worst-case performance.
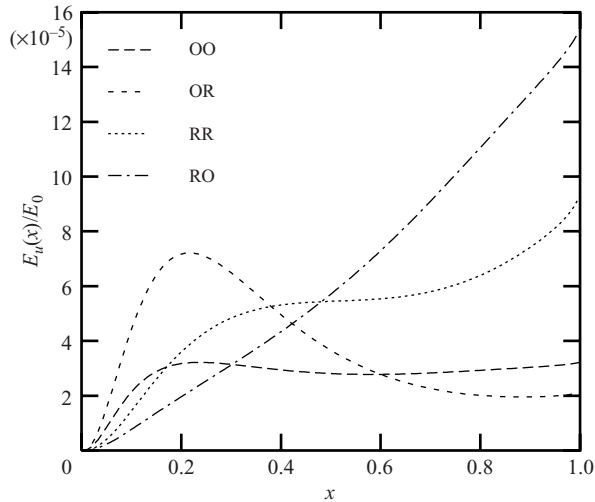
FIGURE 21. Perturbation energy $E_u(x)/E_0$ for $E_0 = 1$, $E_w = 5$, $\beta = 0.8$ and different cases according to table 2.

6. Summary and conclusions

This paper has discussed the optimal and robust control of the steady three-dimensional, algebraically growing instability in the incompressible boundary layer developing nonlinearly over a flat plate, by a perturbation-independent mean-flow modification. An adjoint-based optimization technique has been used, first to determine the optimal control in the presence of a given initial condition, and then to search for the worst possible initial condition in the presence of the corresponding optimal control. The latter procedure consists in the identification of a saddle point of the cost functional in parameter space, as outlined by Bewley *et al.* (2000). The energy metric, whose derivatives we render equal to zero via successive iterations, is the disturbance energy integrated over the whole volume of the fluid. The extremization of a different objective (e.g. the final perturbation energy) produces undesired excursions in the disturbance energy, which could lead to advance transition, as already noted by previous authors.

Results are compared at constant wavenumber, at constant initial or control energy and at the optimal wavenumber, defined as the value of β that maximizes the gain for any given energy.

When an optimal control is sought, the initial condition is fixed at the optimal perturbation computed in Zuccher *et al.* (2004), and the steady spanwise-uniform wall-suction profile that optimally opposes it is determined. The choice of a uniform (in z) control stems from practical considerations of realizability: it is the simplest phase-independent (hence feedback-independent) approach. The most evident common feature of all the tests performed is that the control velocity is always negative (i.e. the optimal control consists of suction only) and concentrated in the proximity of the leading edge.

The curves of the mean gain are shown for varying control energies, wavenumbers and initial energies, in the linear and nonlinear regimes. When the control energy is low, the differences from the uncontrolled cases are not significant, whereas high values of E_w render the curve of the gain lower and flatter. This trend is independent of the initial energy.

Increasing the control energy produces better results (i.e. lower gains), as intuitively expected and smoother suction-velocity profiles. The effect of the control on the flow field is to make the mode-zero velocity profile similar to that of an accelerated boundary layer: as more and more fluid is sucked away from the flow, the mean profile becomes fuller and the boundary-layer thickness decreases.

The control on a short window or on two windows is always less efficient than the case in which suction is applied from the leading to the trailing edge. Both the gain and the maximum value of the suction velocity are higher when a reduced control window is employed. Nevertheless, the loss in gain is acceptable and the general features of the optimal suction profile are preserved.

After investigating the characteristics of optimal control, attention was turned to robust control. In fact, when control is on, the previously computed optimal initial perturbation no longer maximizes the mean gain. Robust control overcomes this difficulty by optimizing the initial perturbation simultaneously with the corresponding wall-suction distribution. The results in this setting exhibit a gain that always exceeds that of the corresponding optimal case, as we would expect since the inlet perturbation applied in robust control is by definition the worst possible one.

The results in the case of robust control differ from the corresponding optimal ones as the control energy E_w becomes larger. For E_w reasonably small, in fact, they look very similar because the weak control employed is not sufficient to strongly alter the flow field. On the contrary, with increasing control effort, more differences arise, especially in the wall-suction distribution. Comparisons reveal that the best control resulting from a robust calculation is usually more uniform in x with a lower peak value than the optimal computation. Moreover, in the robust case, the maximum suction is always applied farther downstream than in the optimal case and the resulting optimal gain G is higher by as much as 84%. For the larger control energies, robust-control suction distributions are surprisingly clustered near one another; this is an unexpected bonus for applications and possible wind-tunnel tests to be conducted on the basis of the control laws computed here.

REFERENCES

AIRIAU, C., BOTTARO, A., WALTHER, S. & LEGENDRE, D. 2003 A methodology for optimal laminar flow control: application to the damping of Tollmien–Schlichting waves in a boundary layer. *Phys. Fluids* **15**, 1131–1145.

ANDERSSON, P., BERGGREN, M. & HENNINGSON, D. S. 1998 Optimal disturbances in boundary layers. *AFOSR Workshop on Optimal Design and Control*, Arlington VA, USA, 30 Sept.–3 Oct. 1997 (ed. J. T. Borggaard, J. Burns, E. Cliff & S. Schreck). Birkhauser.

ANDERSSON, P., BERGGREN, M. & HENNINGSON, D. S. 1999 Optimal disturbances and bypass transition in boundary layers. *Phys. Fluids* **11**, 134–150.

ANDERSSON, P., BRANDT, P., BOTTARO, A. & HENNINGSON, D. S. 2001 On the breakdown of boundary layer streaks. *J. Fluid Mech.* **428**, 29–60.

BEWLEY, T. R. & LIU, S. 1998 Optimal and robust control and estimation of linear paths to transition. *J. Fluid Mech.* **365**, 305–349.

BEWLEY, T., TEMAM, R. & ZIANE, M. 2000 A general framework for robust control in fluid mechanics. *Physica* D **138**, 360–392.

BOIKO, A. V., WESTIN, K. J. A., KLINGMANN, B. G. B., KOZLOV, V. V. & ALFREDSSON, P. H. 1994 Experiments in a boundary layer subjected to free-stream turbulence. Part 2. The role of TS-waves in the transition process. *J. Fluid Mech.* **281**, 219–245.

CATHALIFAUD, P. & LUCHINI, P. 2000 Algebraic growth in boundary layers: optimal control by blowing and suction at the wall. *Eur. J. Mech.* B/*Fluids* **19**, 469–490.

CORBETT, P. & BOTTARO, A. 2001 Optimal control of nonmodal disturbances in boundary layers. *Theoret. Comput. Fluid Dyn.* **15**, 65–81.

FLORYAN, J. M. & SARIC, W. S. 1979 Stability of Görtler vortices in boundary layer with suction. *AIAA Paper* (79–1479). AIAA 12th Fluid and Plasma Dynamics Conf., Williamsburg.

JOSLIN, R. 1998 Aircraft laminar flow control. *Annu. Rev. Fluid Mech.* **30**, 1–29.

KENDALL, J. M. 1985 Experimental studies of disturbances produced in pre-transitional laminar boundary layer by weak free stream turbulence. *AIAA Paper* 85-1695.

KENDALL, J. M. 1998 Experiments on boundary-layer receptivity to free-stream turbulence. *AIAA Paper* 98-0530.

LANDAHL, M. T. 1980 A note on an algebraic instability of inviscid parallel shear flow. *J. Fluid Mech.* **98**, 243–251.

LUCHINI, P. 1997 Effects on a flat-plate boundary layer of free-stream longitudinal vortices: optimal perturbations. *EUROMECH 3rd European Fluid Mech. Conf. Göttingen 15–18 Sept. 1997*, DLR, Göttingen, p. 219.

LUCHINI, P. 2000 Reynolds-number-independent instability of the boundary layer over a flat surface: optimal perturbations. *J. Fluid Mech.* **404**, 289–309.

LUCHINI, P. & BOTTARO, A. 1998 Görtler vortices: a backward-in-time approach to the receptivity problem. *J. Fluid Mech.* **363**, 1–23.

MATSUBARA, M. & ALFREDSSON, P. H. 2001 Disturbance growth in boundary layers subjected to free-stream turbulence. *J. Fluid Mech.* **430**, 149–168.

MYOSE, R. Y. & BLACKWELDER, R. F. 1991 Control the spacing of streamwise vortices on concave walls. *AIAA J.* **29**, 1901–1905.

MYOSE, R. Y. & BLACKWELDER, R. F. 1995 Control of streamwise vortices using selective suction. *AIAA J.* **33**, 1073–1080.

PRALITS, J. O., HANIFI, A. & HENNINGSON, D. H. 2002 Adjoint-based optimization of steady suction for disturbance control in incompressible flows. *J. Fluid Mech.* **467**, 129–161.

SCHLICHTING, H. 1979 *Boundary–Layer Theory*, 7th edn. McGraw-Hill.

SCHMID, P. & HENNINGSON, D. S. 2001 *Stability and Transition in Shear Flows*. Springer.

TREFETHEN, L. N., TREFETHEN, A. E., REDDY, S. C. & DRISCOLL, T. A. 1993 Hydrodynamic stability without eigenvalues. *Science* **261**, 578–584.

WESTIN, K. J. A., BOIKO, A. V., KLINGMANN, B. G. B., KOZLOV, V. V. & ALFREDSSON, P. H. 1994 Experiments in a boundary layer subjected to free stream turbulence. Part 1. Boundary layer structure and receptivity. *J. Fluid Mech.* **281**, 193–218.

WU, X. & CHOUDHARI, M. 2001 Effect of long-wavelength Klebanoff modes on boundary-layer instability. *CTR Annu. Res. Briefs*, 305–316.

ZUCCHER, S., BOTTARO, A. & LUCHINI, P. 2004 Algebraic growth in a Blasius boundary layer: nonlinear optimal disturbances. *Eur. J. Mech.* B/*Fluids* (submitted).